EPITAXIALLY SELF-ASSEMBLED QUANTUM DOTS

Recent progress in lithography, colloidal chemistry, and epitaxial growth have made it possible to fabricate structures in which carriers or excitons are confined in all three dimensions to a nanometer-sized region of a semiconductor. Structures like these are commonly called quantum dots (see the article by Marc A. Kastner in Physics TODAY, January 1993, page 24). The quantum dots that we focus on in this article

Nanometer-scale islands that form spontaneously on a semiconductor substrate have atomlike properties and potential applications in optical and optoelectronic devices, quantum computing, and information storage.

> Pierre M. Petroff, Axel Lorke, and Atac Imamoglu

form spontaneously during the epitaxial growth process, with confinement provided in all three dimensions by a high bandgap in the surrounding material. By contrast, in lithographically defined quantum dots, a quantum well provides a confining potential along the growth direction while the lateral confinement is provided by an electrostatically induced potential barrier. In the past few years, quantum dots have attracted considerable interest because their atomlike properties make them a good venue for studying the physics of confined carriers and many-body effects. They could also lead to novel device applications in fields such as quantum cryptography, quantum computing, optics, and optoelectronics.

The presence of a discrete energy spectrum distinguishes quantum dots from all other solid-state systems and has caused them to be called "artificial atoms." However, the atom-quantum dot analogy should not be carried too far: Unlike electrons in an isolated atom, carriers in semiconductor quantum dots-which contain from a few thousand to tens of thousands of atoms arranged in a nearly defect-free three-dimensional crystal latticeinteract strongly with lattice vibrations and could be strongly influenced by defect, surface, or interface states.

One of the most important consequences of strong carrier confinement in quantum dots is the prominent role of many-particle effects. Coulomb interactions between carriers control the quantum dot charging and

PIERRE PETROFF is a professor in the materials department and ATAC IMAMOGLU is a professor in the department of electrical and computer engineering at the University of California, Santa Barbara. AXEL LORKE is a professor in the Laboratory for Solid-State Physics at Gerhard-Mercator University in Duisburg, Germany.

carrier recombination dvnamics. Some of the manybody effects have already been investigated in lithographically defined quantum dots, including the physics of Coulomb charging and the Kondo effect1 (see PHYSICS TODAY, January 1998, page 17). Measurements of transport properties in a magnetic field have been used to study the filling of energy levels and the validity of Hund's rule in these electrostatically de-

fined quantum dots.2 Unexpected effects have been reported in these systems, including the pairwise loading of electrons into quantum dots.3

Self-assembled quantum dots have smaller sizes and stronger confinement potentials than lithographically defined quantum dots and therefore permit the study of different quantization regimes. Unlike lithographically defined nanostructures, self-assembled quantum dots can be easily fabricated and readily analyzed using optical spectroscopy and measurements of their transport properties. Based on experimental results, it seems likely that self-assembled quantum dots will play a key role in the emerging fields of single-particle electronics and photonics.

Growing quantum dots, rings, and lattices

Fabrication of self-assembled quantum dots begins with some form of atomic deposition onto the surface of a semiconductor substrate, where the deposited material is chosen to have a smaller bandgap than the substrate. During the deposition process, epitaxial islands spontaneously form for energetic reasons on the crystal surface. These islands are then made into quantum dots by covering them with another semiconductor layer having a larger bandgap than the islands.

In practice, in-situ growth techniques such as molecular beam epitaxy or metalorganic chemical-vapor deposition are used to obtain the requisite ultraclean conditions and exquisite control of deposition parameters. With these techniques, a flux of atoms (for example, gallium, indium, or arsenic) is sent onto an ultraclean gallium arsenide surface held at high temperature. After diffusing across the clean reconstructed surface, the atoms arrange themselves, starting from step edges, to form a continuous epitaxial layer. The surface, interfacial, and elastic ener-

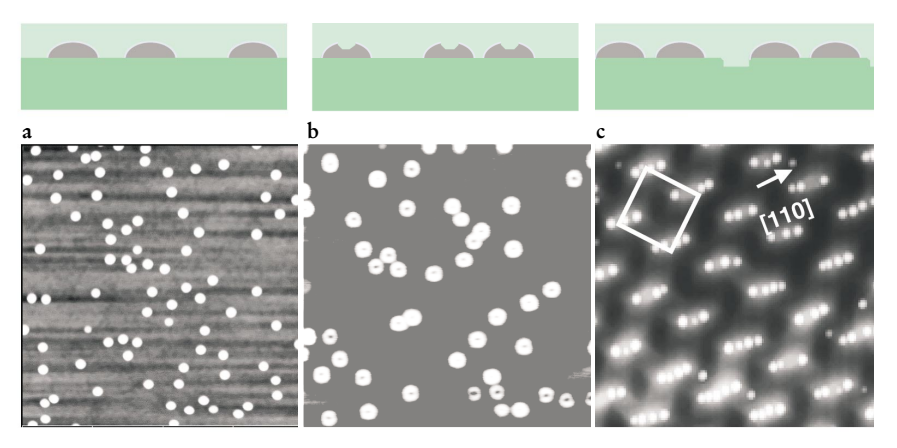


FIGURE 1. ATOMIC FORCE MICROGRAPH images (bottom) of islands epitaxially grown on a gallium arsenide-(001) substrate, and schematics (top) of the profile of the islands showing their shape and distribution. The islands are transformed into quantum dots or rings by covering them with a GaAs epitaxial film (represented by the light shading on the top drawings). The lateral size of each AFM image is 1 μ m, and the quantum dot density is between 5×10^9 cm⁻² and 2×10^{10} cm⁻². (a) Indium arsenide islands are randomly nucleated on the surface. The islands are shaped like truncated pyramids with a base of 30-40 nm and a height of 4-8 nm. (b) In Ga_{1-x}As ring-shaped islands are randomly distributed on the substrate. The depressed center of the ring can be seen as a small black dot in the image. (c) InAs islands on a GaAs substrate form a two-dimensional lattice with a unit cell (indicated in white) containing three to four islands per lattice point. The lattice is formed by patterning the substrate before nucleation with a periodic mesa pattern incorporating localized stress centers under the mesas. Nucleation takes place preferentially on top of the mesas in order to minimize the film energy on the surface and relax local elastic stresses. The number of islands in the basis, the lattice period, and the orientation of the twodimensional lattice of islands can all be adjusted by varying the InAs flux and the size, orientation, and period of the mesa lattice.

gies of the epitaxial film change during the film deposition process and the atomic arrangement on the surface develops so as to minimize the sum of these energies. The elastic strain energy of the film grows quadratically with the film thickness, and if the epitaxial film material has a lattice parameter even a few percent different from that of the substrate, nanometer-sized islands can form on the surface to minimize the total energy. This film relaxation is elastic, so no defects are introduced in the island formation process.

The growth process just described has been used to form In_xGa_{1-x}As quantum dots within a GaAs substrate. Here, the lattice misfit strain varies from 0 to 7% as the In concentration x increases from 0 to 1. As shown by the atomic force micrograph images in figure 1, the growth process for this well-studied system can be controlled to produce new quantum dot shapes, dimensions, and lattices. The usual growth pattern is a random nucleation of islands at step edges on the clean surface, with the quantum dots having a truncated pyramidal shape (figure 1a). Altering growth conditions can cause the islands to form with a ring shape,5 though still in a random array (figure 1b). Remarkably, the random array of

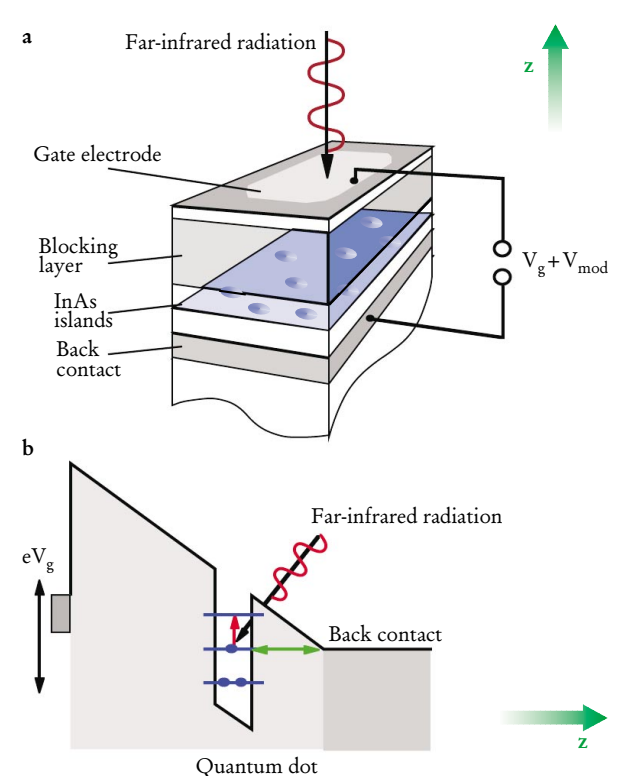


FIGURE 2. QUANTUM-DOT FIELD-EFFECT DEVICE used to probe the electronic states of self-assembled quantum dots and quantum rings. (a) The device consists of a capacitor-like structure between two parallel conducting plates; the self-assembled islands are embedded, as indicated, in an internal layer. The lower plate (back contact) is part of the grown semiconductor structure and consists of a highly (silicon) doped GaAs layer. The top plate is a thin, transparent, metal layer evaporated on top of the sample. The field inside the capacitor structure, and thus the energetic alignment between the islands and the back contact, can be tuned by an external voltage V_a applied between the back contact and the top gate. Because the back contact is located only some tens of nanometers away from the islands, electrons can readily tunnel back and forth between the two if an electronic level in the islands is aligned with the chemical potential of the back contact. When a small AC voltage V_{mod} is added to V_{g} , the resulting shift of charge back and forth between the back contact and the dots will manifest itself by an increased capacitive signal in the external circuit, which can be used for capacitance spectroscopy. (b) A schematic conduction band diagram shows that electrons enter the quantum dots by tunneling from the back gate through the GaAs barrier (the triangular section above the double-headed green arrow). The allowed dipole transitions of the many-particle system are measured using infrared spectroscopy, as indicated: The lower energy level is populated from the back contact using an applied bias (green arrows), then an incident infrared photon induces a transition between two quantum dot energy levels (red arrow), and the transition energy is measured by infrared absorption spectroscopy.

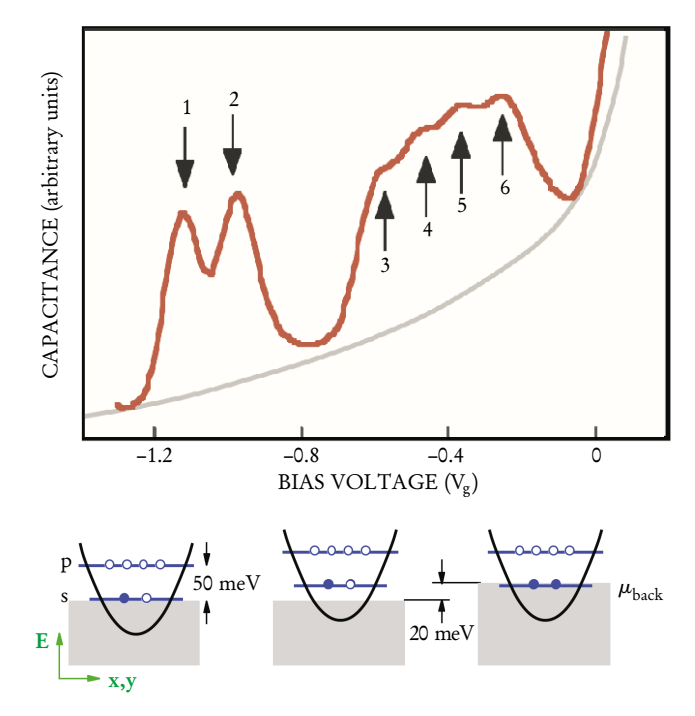


FIGURE 3. CAPACITANCE SPECTROSCOPY reveals quantumdot electron occupancy and ground-state energies in the fieldeffect device shown in figure 2. Above, measured capacitance is plotted as a function of bias voltage V_a . Numbered arrows indicate the peaks that occur where an additional electron enters the dot. Below, the schematic band diagrams show the changes in the effective confining potential (black curve) and in the lowest energy levels (connected blue circles, filled in for occupied levels) as electrons are added to the quantum dot. The Fermi level μ_{back} of the back gate, which is proportional to the bias voltage, is at the top of the dark shading in the diagrams. Although the lowest energy state is doubly spin degenerate, electron-electron interaction makes it harder to load the second electron into a quantum dot than the first. The energy levels when the first electron enters the dot are shown at bottom left; Coulomb interaction raises the energy of the two-electron state by almost 20 meV compared to the one-electron state (the so-called Coulomb blockade), as shown at bottom center. To load the second electron the back gate potential must be raised (bottom right). Adding a third electron would require both the Coulomb energy and the quantization energy of about 50 meV, so there is a gap in voltage between the second and the third peak in the charging characteristic (top). To convert from bias voltages to energies, a scaling factor (about 7 for the present structure) is used, which can be derived from a simple evaluation of the capacitative energy at the quantum dot layer.

islands can be changed into a periodic one by controlling the quantum-dot nucleation on the surface (figure 1c).⁶

The island structures depicted in figure 1 are converted to quantum dots by covering them with a GaAs epitaxial layer. A 3D array of quantum dots can then be produced by repeating the deposition sequence just described. If the distance between successive InAs layers is less than about 10 nm, the quantum dots in successive layers tend to be aligned in order to minimize the elastic strain energy of the InAs layers.⁴ This vertical strain coupling has recently been exploited to construct a 3D quantum-dot crystal,⁶ starting with a 2D template like the

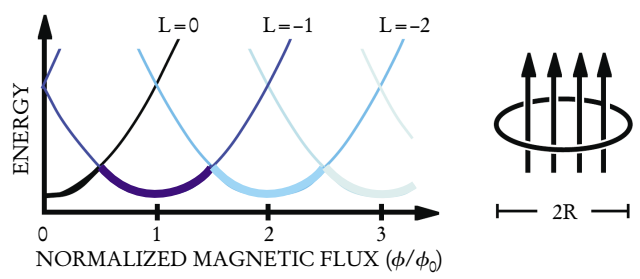


FIGURE 4. QUANTUM-RING ENERGY STATES are a function of the external magnetic field because the magnetic flux penetrates the ring, as shown at right. Periodic boundary conditions make the energy states a function of an integer L; whereas for quantum dots the ground state always has L=0, for quantum rings with a nonzero magnetic field the ground state could have nonzero L values. Plotted at left is the calculated energy of a simple model of a quantum ring for several L values as a function of the flux through the ring normalized to the flux quantum $\phi_0 = h/e$; the ground state as a function of flux is indicated by the heavy line.

array shown in figure 1c.

Epitaxial growth and the chemistry of interfaces are complex subjects, and major challenges remain for improving size uniformity and controlling the composition, position, and shape of quantum dots. Nevertheless, a wide variety of quantum-dot systems has been made using the epitaxial growth approach, including group IV elemental systems (such as Si–SiGe), and group II–IV and III–V compound semiconductors.

Electronic properties of dots and rings

In contrast to real atoms, for which the confining Coulomb potential is well known, the forces that keep the carriers in place in self-organized islands are difficult to estimate from first principles. The exact shape and composition of the islands are not well known and depend on the growth procedure; in addition, complications are introduced by the complex band structure of the strained material and the effect of piezoelectric forces.7 Studies often define an effective confining potential inside the dots or rings; a good assessment of this quantity can be obtained from a combined study of the ground-state and excitation energies. Ground-state energies are investigated by capacitance spectroscopy.8 Excitations can be studied by transmission spectroscopy in the far infrared⁸ (see the article by Detlef Heitmann and Jörg P. Kotthaus in PHYSICS TODAY, June 1993, page 56). For self-assembled quantum dots and rings, both kinds of spectroscopic measurements can be made with a special field-effect structure, shown in figure 2, that is based on a metal-insulator-semiconductor field-effect transistor (MISFET) design.

The capacitance—voltage characteristic of quantum dot samples typically manifests six maxima, as shown in figure 3, where the indicated maxima denote the loading of one through six electrons into the dot. The charging peaks are grouped according to the internal shell structure in the dots, which is indicated at the bottom of figure 3. The first two electrons fill the lowest, spin-degenerate state, the so-called s shell. The fact that the next shell consists of four roughly equally spaced maxima is a direct consequence of the shape of the confining potential, with symmetry in the xy plane and much stronger confinement along the growth direction z because of the oblate shape of the self-assembled islands. It turns out that many elec-

tronic properties of quantum dots can be well accounted for by assuming parabolic confinement in the *xy* plane.

After the charging state has been determined by capacitance spectroscopy, far-infrared spectroscopy can be used to study the excitations of the n-electron state in the dots. As long as only the s state is filled (n = 1, 2), the far-infrared data agree well with the parabolic model and allow for a precise determination of the effective curvature of the confining potential. When the third electron is loaded (a state corresponding to "quantum dot lithium"), the character of the spectrum changes and the simple parabolic model no longer explains the data. The process just described can be used to investigate the quantum-dot "periodic table," with each element exhibiting a characteristic spectroscopic fingerprint.

In many respects, quantum rings are just quantum dots with a peculiar (*w*-shaped rather than par-

abolic) confining potential. The decisive difference in their topology—the "hole" in their middle—becomes prominent when an external magnetic field is applied. The magnetic flux that penetrates the interior of the ring will then determine the nature of the electronic states.

The energy states in quantum rings can be most easily derived by assuming the rings to be an infinitely thin wire bent into a loop of radius R. This system is a textbook case of a one-dimensional solid with periodic boundary conditions. The energy spectrum is readily calculated to be

$$E_L = \frac{\hbar^2 k_L^2}{2m} = \frac{\hbar^2}{2mR^2} L^2, \quad L = 0, \pm 1, \pm 2, ...,$$

where m is the mass of the electron. When the quantum ring is placed in a magnetic field, the phase shift picked up by the electron on its way around the ring leads to an additional term, which involves the ratio between the flux through the ring ϕ and the flux quantum $\phi_0 = h/e$. With a magnetic field, the quantum ring energy spectrum becomes:

$$E_L = \frac{\hbar^2}{2mR^2} \left(L + \frac{\phi}{\phi_0} \right)^2.$$

The resulting energy dispersion, a set of parabolas shifted along the magnetic field axis according to the respective L value, is shown in figure 4. If the magnetic field increases above the level corresponding to $\phi/\phi_0=\frac{1}{2}$, the ground state (lowest energy state) will shift from the L=0 to the L=-1 parabola. A similar change in ground state will take place for each additional flux quantum in the interior of the ring. This results in an Aharonov–Bohm-type periodic oscillation in the ground-state energy, as can be seen by following the thick lines in figure 4 that mark the actual ground state.

The nonvanishing angular momentum of quantum rings in the presence of a magnetic field is closely related to the fascinating physics of the so-called persistent currents in mesoscopic rings. ¹⁰ Unlike mesoscopic rings, however, self-assembled InGaAs rings function in the true,

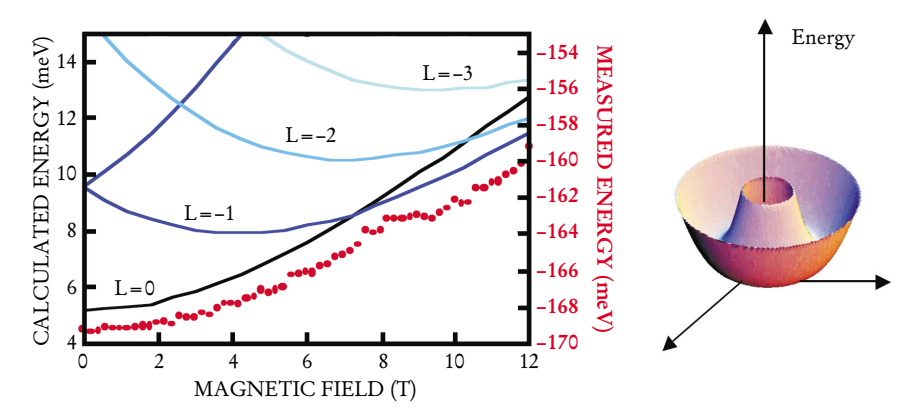


FIGURE 5. ELECTRON ENERGY LEVELS for a magnetized quantum ring are plotted as a function of magnetic field. The solid lines plot computed energies for an idealized ring using parameters (width, radius) that were estimated from far-infrared spectroscopy of actual rings. The different lines are parametrized by the integer L, which is related to the angular momentum of the state. The ground-state energy at a given magnetic field is the minimum energy of any of the colored lines; note the change in ground state from the L=0 to the L=-1 line at 8 tesla. The red dots (plotted with the right-axis scale) give the measured energy of the level, based on the positions of the lowest charging maximum in the capacitance. The illustration at right shows the shape of the confining potential used in the calculation.

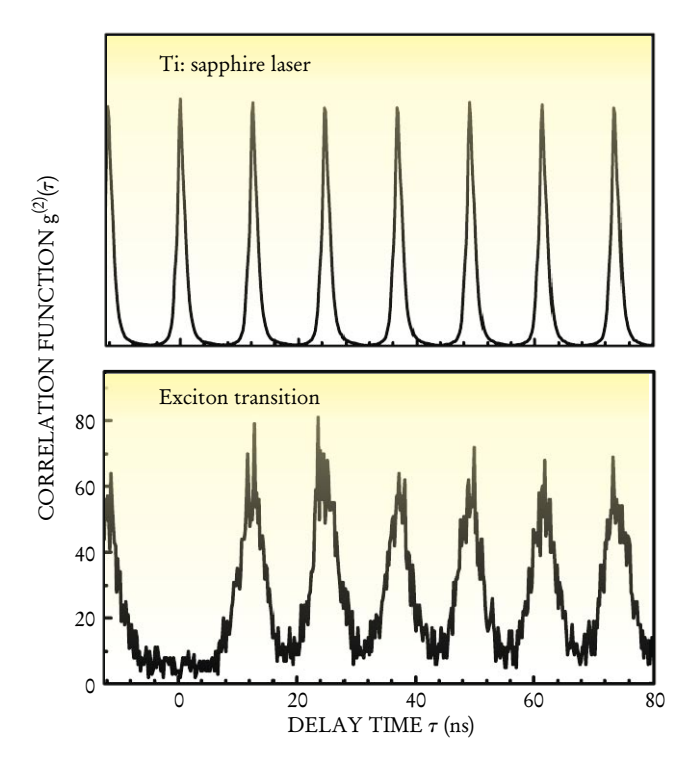
scatter-free, quantum limit, and they are therefore more like ring-shaped molecular systems such as benzene. Note, however, that trapping a flux quantum inside benzene would require a magnetic field of about 8×10^4 T, many orders of magnitude stronger than those available in today's laboratories.

The quantum-dot single-electron ground state will always have L=0, and so the change in ground state from L=0 to L=-1 is a decisive feature distinguishing quantum rings from quantum dots. Far-infrared spectroscopy of samples with ring-shaped islands suggests that such a ground-state transition takes place at a magnetic field of close to 8 T. At this field, the excitation spectrum is observed to undergo a drastic change, with new resonances appearing and others disappearing. The conjecture that this behavior is caused by a change in ground state can be tested experimentally with capacitance spectroscopy, where the single-particle ground state can be directly monitored by mapping out the position of the lowest charging maximum as a function of the magnetic field.

Figure 5 shows the calculated energy states of a model quantum ring having dimensions that are based on an evaluation of experimental far-infrared data; the red data points give the measured magnetic-field dispersion of the lowest charging peak. The kink in the data-point curve at 8 T matches the cusp in computed ground-state energy and confirms that, at this magnetic field, the ground-state L value changes. These data also indicate that the ring shape of the uncovered InGaAs islands is indeed translated into a not-simply-connected electronic state.

Quantum-dot cavity quantum electrodynamics

Cavity quantum electrodynamics (cavity QED) has provided an invaluable tool for investigating quantum phenomena (see the article by Serge Haroche and Daniel Kleppner in Physics Today, January 1989, page 24 and the article by Yoshihisa Yamamoto and Richart Slusher in Physics Today, June 1993, page 66). This field of atomic physics and quantum optics has shown, for example, that spontaneous emission of radiation from excited atoms can



be greatly enhanced or inhibited by placing the atoms in a specially designed cavity or between mirrors. Modification of spontaneous emission due to the presence of a cavity is known as the Purcell effect.

The elementary system in cavity QED is a two-level system interacting with a single cavity mode. 11 If the electric field per photon inside the cavity is sufficiently large, then the exchange of energy between the two-level emitter and the cavity mode will be reversible and the cavity will have a strong effect on the two-level system. To reach this so-called strong-coupling regime of cavity QED, the single-photon Rabi frequency g must exceed the decoherence rates in the system from cavity losses and dipole dephasing. This means that for a two-level emitter with a large optical dipole moment, the cavity structure must have an ultrasmall optical mode volume and a high quality factor Q.

A ground-state exciton in a self-assembled quantum dot constitutes an ideal two-level system for cavity QED applications. Unlike atoms, quantum dots do not undergo random motion; they are naturally trapped in the surrounding high-bandgap-energy semiconductor. The advanced semiconductor fabrication techniques used for quantum dots can be used to shape the semiconductor material in which the quantum dots are embedded so that the resulting photonic structure supports high-Q optical modes with mode volumes approaching the fundamental limit determined by the wavelength of the generated photon.

One of the principal applications of cavity-QED techniques has been in the emerging field of quantum information science: A significant fraction of quantum computation and communication schemes rely on the strong-coupling regime of cavity QED.¹² It is possible to enhance the total radiative decay rate of the emitter by using a cavity and the Purcell effect, even when the dipole coupling rate is smaller than the cavity decay or dipole-dephasing rates.¹³ If the cavity mode has a preferential output direction, the Purcell effect will ensure fast and directional emission from the two-level system. These features are

FIGURE 6. INTENSITY CORRELATION FUNCTION for a quantum-dot single-photon source based on pulsed laser excitation of a single quantum dot embedded in a microdisk. Plotted are the correlation function for the titanium-sapphire excitation laser (top) and quantum-dot ground-state emission under excitation conditions (bottom), as a function of the time delay τ between the photon arrival times (see the box on page 51). The absence of a peak at $\tau=0$ in the emission correlation function shows that none of the pulses contains more than one photon. (Adapted from ref. 15.)

highly desirable for applications in optoelectronics as well as in quantum information.

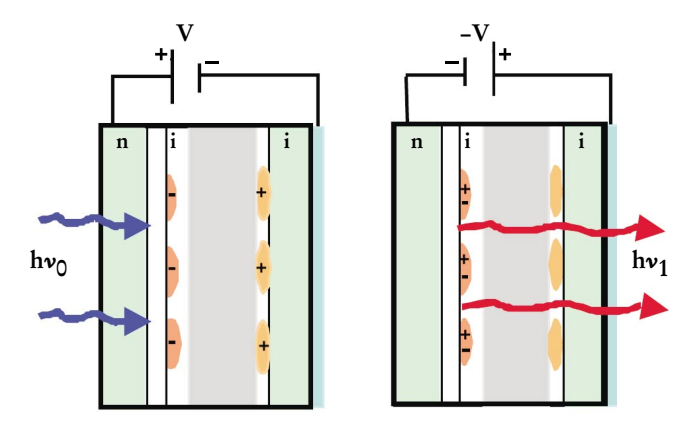
Experiments on quantum dots embedded in micropillar and microdisk structures have already demonstrated the Purcell effect, both for an ensemble of dots13 and for a single dot. 14 Observations in quantum dot-microdisk structures of high-Q whispering gallery modes—spherically symmetric resonant-cavity modes where the electromagnetic energy is concentrated mostly on the periphery—suggest that the strong-coupling regime could be reached in this system.¹⁴ In photonic bandgap (PBG) materials, which are periodic structures that forbid photon propagation in a particular frequency range, progress has been slower due to the significantly more demanding processing required. On the other hand, recent experiments on quantum dots embedded in 2D PBG defect cavities indicate that this system is likely to play a dominant role in cavity QED with quantum dots in the near future.

A major success of quantum-dot cavity QED—and an indication of the great potential of self-assembled quantum dots for applications in quantum information technology—is the realization of a quantum-dot single-photon turnstile device. Photon correlation measurements (see the box on page 51) on a single quantum dot embedded in a microdisk have revealed that, when saturated, this dot generates one-and only one-photon at the fundamental exciton transition for every excitation pulse from a modelocked laser. The result was an 82-MHz repetition rate single-photon source. 15 The intensity correlation function for this device is shown in figure 6 along with that for the excitation laser. Absence of a peak in the photon source correlation function at zero time delay indicates that the probability of emitting a pulse containing two or more photons is negligible. The microdisk cavity is an important component of the device: When the quantum-dot fundamental exciton line is on resonance with a cavity mode, the Purcell effect shortens the radiative recombination time and improves the collection efficiency. Such a source is predicted to be a key ingredient in quantum cryptography and could enable quantum computation using only linear optical elements.

Quantum-dot information storage

Trapping carriers in a quantum dot prevents diffusion or drift and can drastically reduce the carriers' rate of recombination with ionized impurities or other defects. This effect can be used as the basis for a very-high-density memory device in which information is written and read by controlling charge storage in quantum dots.¹⁶

Such a charge-storage memory device that uses light for reading and writing information is shown schematically in figure 7. An incident photon representing a data point generates an exciton that is dissociated within the



structure into an electron and hole, which are then stored in a pair of closely spaced, strain-coupled quantum dots. The induced dipole resulting from the electron and hole separation is detectable by luminescence. The when the stored information is to be read, the exciton can be reassembled by using an applied electric field to drive the hole into the quantum dot that contains the stored electron. Monitoring the light output from the device as a function of storage time gives a measure of the charge storage capability. Charge storage times of up to 10 s have

FIGURE 7. A QUANTUM-DOT MEMORY DEVICE based on controlled charge storage. Two strain-coupled quantum-dot layers are fabricated within a field-effect transistor with an n+ gallium arsenide-type doped back gate and a gold semitransparent Schottky front gate. The quantum-dot layers (light green) are separated by a thin aluminum arsenide layer (gray) that permits very fast (about 0.5 ps) electron transfer. (a) For the write cycle, a photon-induced exciton is dissociated by the internal field into an electron and hole pair, which are stored, respectively, in an indium arsenide quantum dot and in a nearby strain-induced GaAs quantum dot. (b) The information is read optically by applying a positive voltage pulse to the front Schottky contact, which drives the hole from the straininduced quantum dot into the quantum dot containing the electron. The exciton is regenerated and recombines to emit a photon, which is then observed using standard photon-detection techniques.

been measured, which are remarkably long when compared to the exciton lifetime in a quantum dot of about 5 ns. ¹⁸ The idea behind this device—dissociating an exciton for storage in a quantum-dot pair and then reassembling it for readout—could turn out to be a viable approach for an all-optical memory.

Optically addressing a single quantum dot using a

Photon Correlation Measurements

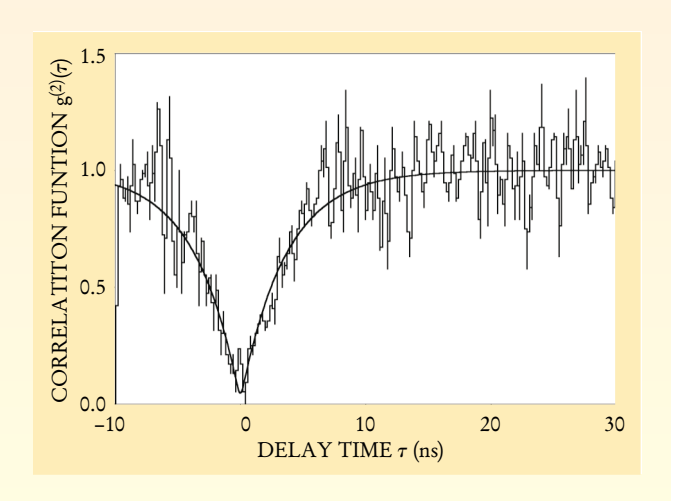
Since the pioneering experiments by Robert Hanbury-Brown and Richard Q. Twiss, photon correlation measurements have become a major tool in quantum optics and the spectroscopy of single-quantum systems.¹¹ Such experiments measure the likelihood that, given an initial photon detection event at time t, a second photon will be detected at time $t + \tau$. The experimental setup consists of a 50/50 beamsplitter and two single-photon counting avalanche photodiodes (SPADs), each of which generates a voltage pulse upon detection of a single photon. The pulses from the two SPADs are used to start and stop a time-to-amplitude converter, which translates the time delay between the start and stop pulses into a voltage amplitude. The result is a count of the number of pairs of photons $n(\tau)$ that have an arrival-time separation of τ . In the limit where the reciprocal of the average counting rate is much longer than the monitored time range, $n(\tau)$ is proportional to the normalized intensity correlation function $g^{(2)}(\tau)$. 11

For a coherent light source, such as a single-mode laser, $g^{(2)}(\tau)=1$. Physically, this means that detection of a photon at time $\tau=0$ gives us no information about the succeeding photon-detection event; that is, the photons that make up a coherent light beam are completely uncorrelated. If, on the other hand, a light source satisfies either $g^{(2)}(0) < g^{(2)}(\tau)$ or $g^{(2)}(0) < 1$, this indicates that two photons are unlikely to appear simultaneously at the detectors. The first observation (in 1977) of this "photon antibunching" in fluorescence from a single atom has been generally regarded as the first proof of the quantum nature of light, since these correlations cannot be explained without quantizing Maxwell's equations.¹¹

Fluorescence from a single anharmonic quantum emitter has the property that $g^{(2)}(0) \approx 0$. This strong quantum correlation among photons is easily washed away with an increasing number of emitters. We can therefore consider strong photon antibunching ($g^{(2)}(0) < 0.5$) as direct evidence that the source of the radiation field is a single-emitter quantum sys-

tem. In contrast, observation of sharp emission peaks in photoluminescence spectra is not sufficient to rule out the presence of two or more identical emitters.

Photon correlation measurements have recently been carried out in both colloidal and self-assembled quantum dots. The figure shows the measured intensity correlation function of the fluorescence from the fundamental exciton line of a single self-assembled quantum dot. The dip at zero time delay is direct evidence that the fluorescence comes from a single anharmonic quantum emitter. The time scale on which the correlation function changes from $g^{(2)}(0) \approx 0$ to $g^{(2)}(\tau) \approx 1$ is ultimately determined by the single-exciton recombination time. Thus, in addition to confirming the prior photoluminescence-based identification of single quantum-dot exciton lines, these measurements are also useful as a spectroscopic tool for measuring quantum-dot recombination times without requiring mode-locked laser sources for excitation.



microphotoluminescence microscope has become routine in the past few years. With improvements in quantum-dot ordering and positioning, we can hope in the near future to address and store information optically in a single quantum dot, thus opening the possibility of ultrahigh-density memory devices.

With self-assembled quantum dots, quantum control of carrier injection and photon generation is now possible. The experiments discussed and referenced in this article demonstrate the immense potential of this type of quantum dot for enabling new science and technology. Especially notable is the key role that quantum dots are likely to play in the emerging field of quantum-information science—either as building blocks where quantum information is stored in the spin degrees of freedom, or as a source of single photons for quantum communication.

On the other hand, our understanding and control of quantum-dot growth and physics are far from complete. Reducing the quantum-dot size distribution and the observation of 3D confinement effects at room temperature remain outstanding challenges for materials science. Further research in these areas should yield a wealth of new physical phenomena and exotic devices.

This research has been supported by the US Army Research Office, the Air Force Office of Scientific Research, the Defense Advanced Research Projects Agency, the National Science Foundation and a David and Lucile Packard Fellowship (Atac Imamoglu). The authors also acknowledge the numerous and invaluable contributions of their colleagues at the University of California, Santa Barbara, and in the solid-state physics group at the Ludwig Maximilian University in Munich, Germany.

References

- 1. D. Goldhaber-Gordon et al., Nature 391, 156 (1998).
- S. Tarucha, D. G. Austing, T. Honda, R. J. van der Hage, L. P. Kouwenhoven, Phys. Rev. Lett. 77, 3613 (1996).
- N. B. Zhitenev, R. C. Ashoori, L. N. Pfeiffer, K. W. West, *Phys. Rev. Lett.* 79, 2308 (1997).
- D. Leonard et al., Appl. Phys. Lett. 63, 3203 (1993). J.-Y. Marzin et al., Phys. Rev. Lett. 73, 716 (1994). Q. Xie, A. Madhukar, P. Chen, N. P. Kobayashi, Phys. Rev. Lett. 75, 2542 (1995).
- 5. J. M. Garcia et al., Appl. Phys. Lett. 71, 2014 (1997).
- H. Lee et al., Appl. Phys. Lett. 78, 105 (2001). G. Springholz,
 V. Holy, M. Pinczolits, G. Bauer, Science 282, 734 (1998).
- D. Bimberg, M. Grundmann, N. N. Ledentsov, Quantum Dot Heterostructures, Wiley, New York (1998) and references therein.
- H. Drexler et al., Phys. Rev. Lett. 73, 2252 (1994). R. C. Ashoori, Nature 379, 413 (1996). R. Luyken et al., Appl. Phys. Lett. 74, 2486 (1999). G. Meideiros et al., Phys. Rev. B 55, 1568 (1997).
- R. J. Warburton et al., Nature 405, 926 (2000). A. Lorke et al., Phys. Rev. Lett. 84, 2223 (2001).
- M. Büttiker, Y. Imry, R. Landauer, Phys. Letters A 96, 365 (1983)
- D. F. Walls, G. J. Milburn, Quantum Optics, Springer, New York (1994).
- 12. See the special focus issue on experimental proposals for quantum computation: *Fortschr. Phys.* **48** (9–11) (2000).
- J. M. Gerard, B. Sermage, B. Gayral, B. Legrand, E. Costard,
 V. Thiery-Mieg, Phys. Rev. Lett. 81, 1110 (1998).
- 14. P. Michler et al., Nature 406, 968 (2000).
- 15. P. Michler et al., Science 290, 2282 (2000).
- G. Abstreiter et al., Jpn. J. Appl. Phys. 38, 449 (1999).
 G. Yusa, H. Sakaki, Appl. Phys. Lett. 70, 345 (1997).
- T. Lundstrom, W. Schoenfeld, H. Lee, P. M. Petroff, *Science* 286, 2312 (1999).
- 18. E. Dekel et al., Phys. Rev. B 61, 11009, (2000).